Structures 35 (2022) 1125–1137

Contents lists available at ScienceDirect

Structures

journal homepage: www.elsevier.com/locate/structures

Geometric optimisation analysis of Steel–Concrete hybrid wind turbine towers

Xiaogang Huang [a,b], Bikun Li [c], Xuhong Zhou [a,b], Yuhang Wang [a,b,*], Ronghua Zhu [b]

[a] School of Civil Engineering, Chongqing University, Chongqing 400045, China
[b] Yangjiang Offshore Wind Energy Laboratory, Guangdong 529533, China
[c] Department of Physics, Virginia Tech, Blacksburg, VA 24061, USA

ARTICLE INFO

Keywords:
Steel-concrete structure
Hybrid structure
Geometric optimisation
Design equations
Sensitivity analysis

ABSTRACT

Steel–concrete hybrid towers have been proposed for onshore tall wind turbine tower installations. Their bottom sections are built with concrete and top sections with steel. The primary advantages of such hybrid towers include construction using low-cost durable material and avoidance of transport barriers associated with all-steel towers. In this study, a set of design constraints governing the geometry of hybrid towers was proposed to determine the optimal combination of concrete and steel sections. The primary constraint in tower design involves avoiding resonance because a resonant response can significantly damage the tower and trigger turbine fault conditions. A sensitivity analysis was conducted to explore the correlation between the natural frequency and geometry of a tower. The results demonstrated that an increase in the proportion of concrete can lead to a pronounced effect on the first modal frequency of taller towers. Additionally, geometric optimisation was performed on a 160 m tall tower. This resulted in a 12.7% reduction in the total cost compared with that of the initial design.

1. Introduction

Wind power is one of the fastest-growing renewable energy technologies worldwide [1]. Wind turbines are typically supported at high above-ground levels to harness strong wind resources from available sites and provide sufficient rotating space for long blades [2]. Currently, industries that utilise wind energy are facing intense price competition from industries that utilise traditional fossil energy sources. Strategies aimed at increasing hub heights [3–5] have been proposed to maximise energy capture per turbine. As the hub heights and turbine sizes increase, the support structure should be strengthened by widening the tower diameter and increasing the plate wall thickness to resist the increasing design force.

Tubular steel towers are the most common support structures [6–8]. As the hub height and weight of the turbines increase, the prefabricated steel tower approaches its design limits. The tower diameter is limited to 4.3 m, which is dictated by the overpass heights of the highways and railway lines. Furthermore, the thickening of the plate walls is limited by the rolling equipment and fluctuating steel prices.

Different structural configurations [9–20] have been proposed to avoid transport and fabrication challenges in all-steel towers. Alternative tower designs may use high strength concrete or ultra-high-performance concrete, or can offer more efficient combination of steel and concrete, such as concrete filled steel tube. One prevalent approach in China is to construct a hybrid tower comprising an upper tubular steel section and a lower hollow concrete section, as shown in Fig. 1. The steel–concrete hybrid tower (SCHT) offers an opportunity for using low-cost material in larger diameter sections. The concrete segments can also be precast with transportable sizes to avoid transport challenges associated with prefabricated steel towers. Hence, it will be more cost-effective to use a hybrid design compared to the pure steel tubular option as hub heights become taller and wind turbines become heavier.

The designing of a SCHT entails structural analysis using a finite element model (FEM) [21–27] because of its complex geometry. Paredes et al. [21] developed a phenomenological constitutive model to consider the gap opening and gap closing effects in the horizontal joints of a concrete tower. Ghaemmaghami et al. [22] created fine mesh models to evaluate the effectiveness of annular tuned liquid dampers in reducing the structural response of a SCHT. Kenna and Basu [23] proposed a composite model of shell concrete elements and bar tendon elements to investigate the effects of varying key design parameters such as prestress and concrete compressive strength. Ma and Meng [24] developed an

* Corresponding author.
E-mail address: wangyuhang@cqu.edu.cn (Y. Wang).

https://doi.org/10.1016/j.istruc.2021.08.036
Received 27 July 2021; Received in revised form 9 August 2021; Accepted 9 August 2021
Available online 20 August 2021

(a) HaiZhuang (b) POWERCHINA HuaDong

Fig. 1. On-site photos of hybrid towers in China.

optimisation method by employing ABAQUS and a genetic algorithm for pure concrete towers. FEM in a commercial software can offer an accurate representation of complex tower loading and unloading behaviour. However, the FEM requires a significant amount of computation time and analyses. Hence, it is potentially not practical to conduct a full parametric evaluation to realise an optimal design an SCHT.

Previous studies on tower optimisation [28–35] do not provide detailed guidelines for SCHT design. In this paper, a set of design equations governing the tower geometry is presented as a replacement for an FEM, to rapidly determine the geometric properties of an SCHT at the initial design stage. The design constraints can be used with optimisation algorithms to determine the optimised geometry and satisfy the design principles. We conducted sensitivity analyses for the primary constraint to explore the effects of the concrete portion on SCHTs of different heights. By considering the high sensitivity of the first modal frequency to the concrete portion of tall towers, a 160 m high tower was selected to illustrate the effectiveness of the geometric optimisation framework.

2. Overview of the hybrid tower

The SCHT comprises a lower portion built with concrete and an upper portion built with tubular steel, as shown in Fig. 2. The advantages of using concrete over steel are related to low prices worldwide and versatility in terms of production and transport. The steel portion comprises different hollow steel sections welded together; the concrete portion is constructed by manufacturing hollow components in precast plants, which are then transported to the construction site for assembly. The concrete portion is erected in situ by stacking precast segments on top of each other. This stacking process is similar to that adopted when constructing post-tensioned (PT) bridge structures [36,37]. After the horizontal joints between the concrete segments are grouted with mortar, the concrete portion is clamped together via vertical PT tendons.

The pre-stressing tendons are the only continuous reinforcements between adjacent segments. Hence, they are the only reinforcements for providing flexural resistance to the concrete portion of the tower. The concrete portion is anchored at the top end in an adapter ring and at its bottom end in the foundation. The tendons are initially stressed to a level that maintains sufficient force to counteract the tensile stress resulting from bending moments under the applied load. Tendons are typically arranged symmetrically and externally with respect to the concrete wall to avoid torsional effects after stressing. This in turn provides easier access to their assembly.

When designing an SCHT, a number of design cases should be considered to include the worst loading conditions in the service limit state (SLS), ultimate limit state (ULS), and fatigue limit state (FLS) [38–40]. An SCHT is analysed for SLS to ensure its normal use under operational loads. Excessive deformations and vibrations that affect turbine operations are not allowed according to the design of SLS. Furthermore, FLS corresponds to failure due to the effect of dynamic loading, and thus, a fatigue analysis is conducted to verify that structural components exhibit adequate strength to resist cumulative damage. Additionally, the ULS corresponds to the maximum load-carrying resistance, and the structural safety of the SCHT is satisfied by providing adequate resistance.

The structural design of an SCHT historically adopts an iterative procedure as shown in Fig. 3. Throughout the preliminary phase, a trial design is typically selected based on engineering judgement and past

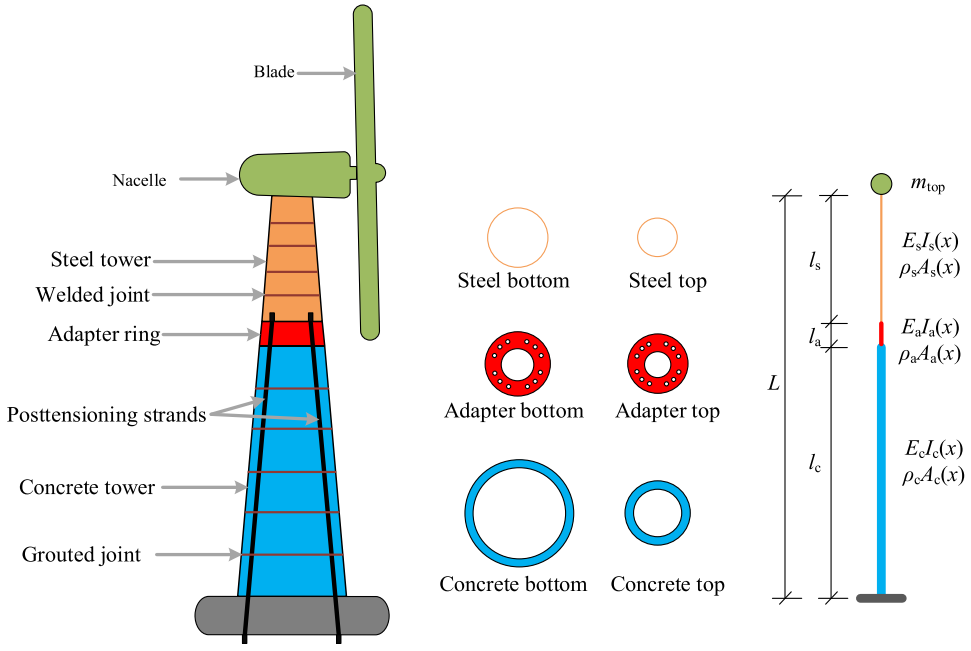

Fig. 2. Conceptual drawing showing the hybrid tower configuration.

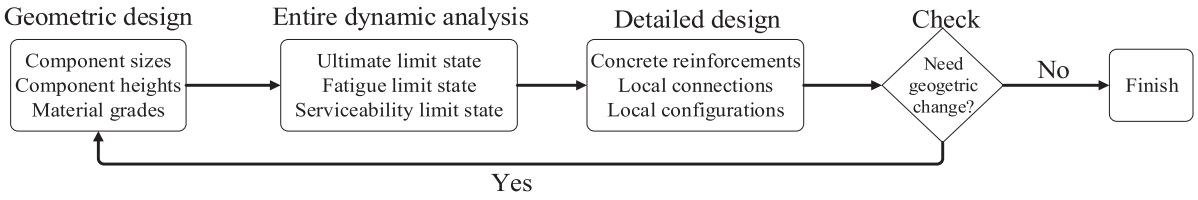

Fig. 3. Flow chart for the design procedure of a hybrid tower.

experiences with respect to the geometry and size of the components. Characteristic values of the material properties are taken in accordance with the relevant standards [40,41]. After the load–resistance responses of the SCHT are evaluated via FEM simulation [41], tower geometric parameters are selected for further dynamic load analysis of the complete system using complex software simulations coupled with nonlinear structural and fluid dynamic models. Dynamic simulation is excessively time-consuming because of the variable wind loading and the complexity of the entire system, starting from the wind turbine to the support structure. In this design step, a 1D beam model was used to represent a complete SCHT system with computational simplicity. However, the simple beam model cannot account for local connections and does not provide detailed stress distributions. Finally, concrete reinforcements, local connections, and configurations of the SCHT were designed in detail based on the dynamic responses. The geometric parameters of the tower were modified if certain design criteria were not satisfied. Any changes in the sizes of the tower components can significantly affect the results of the entire dynamic simulation. Therefore, the design of the SCHT was refined and finalised via an iterative trial-and-error process.

3. Geometric design procedure

A preliminary optimal tower geometry should be selected to avoid low efficiency in the iterative empirical procedure described above. We proposed to preliminarily determine the geometric parameters of the SCHT by using a set of design equations. The five constraints that govern complex geometry of hybrid towers include geometric, frequency, top deflection, compressive stress, and fatigue constraints. The shear constraint was not considered in the framework. This is because shear loads are not critical in the design of slender structures and shear resistance is primarily affected by certain local configurations such as the coefficient of friction across the joints.

For land-based wind energy technology, the support structure is simply a tower that is cantilevered to the ground. Hence, the SCHT can be idealised into a clamped-free beam with flexural stiffness $m(x)$ and mass $n(x)$ per unit length wherein both parameters vary with respect to position $\times$ along length L. The flexural stiffness $m(x)$ and mass $n(x)$ per unit length are expressed as follows:

$$m(x) = m_{\text{top}}\delta(x-L) + \begin{cases} \rho_c A_c(x), & 0 \leqslant x \leqslant l_c \\ \rho_t A_t(x), & l_c \leqslant x \leqslant l_c + l_t \\ \rho_s A_s(x), & l_c + l_t \leqslant x \leqslant L \end{cases} \tag{1}$$

$$n(x) = \begin{cases} E_c I_c(x), & 0 \leqslant x \leqslant l_c \\ E_t I_t(x), & l_c \leqslant x \leqslant l_c + l_t \\ E_s I_s(x), & l_c + l_t \leqslant x \leqslant L \end{cases} \tag{2}$$

where m_{top} denotes the lumped mass at the free end of the beam; and ρ_c, ρ_t, and ρ_s denote the material density of the concrete portion, adapter ring, and steel portion, respectively. Correspondingly, E_c, E_t, and E_s denote material modulus of elasticity, and l_c, l_t, and l_s denote lengths of each portion. A rounded section is the most suitable design for the tower from a mechanical perspective because it can resist the same load from an arbitrary direction. The area and moment of inertia of an arbitrary thin hoop are calculated as follows:

$$A(x) = \frac{\pi[d_o^2(x) - d_i^2(x)]}{4} \tag{3}$$

$$I(x) = \frac{\pi[d_o^4(x) - d_i^4(x)]}{64} \tag{4}$$

where d_o and d_i denote outer and inner diameters.

3.1. Determining the potential tower design space

Manufacturing and transport limitations are primary challenges in building tall wind towers. The geometric constraints applied to the key design parameters of the SCHTs are summarised in Table 1. The maximum diameter of the steel part is limited to approximately 4.3 m, and it is dictated by highway and railway overpass heights. The steel top diameter was varied in a small range of 3300–3500 mm to ensure that a nacelle can be installed on the top tower section. A maximum thickness of 40 mm was assumed for the steel tower given the complexity of the thicker steel fabrication. Based on a field investigation of different SCHTs in China, the concrete portion was tapered from a diameter of 5000–10,000 mm at the base to a diameter of 4800–5500 mm at the top with wall thickness varying in the range 200–400 mm The length ratio of the steel to the concrete portion significantly varied from 0.08 to 1.55. The bottom and top diameters of the adapter were selected to connect the adjacent steel and concrete sections. An adapter ring with a height of 1500–2000 mm and thickness of 1500–1800 mm was fabricated from concrete and was used to decrease the use of steel.

3.2. Deriving equations governing free vibrations

The tower should be designed with sufficient separation between the natural frequencies and turbine operational frequencies of the tower. The operational frequencies include rotor operational frequency (1P) and blade pass frequency (3P for a three-blade turbine). The operational speed of the rotor in different multi-megawatt turbines is approximately 7 to 12 revolutions per minute (rpm) corresponding to a 1P frequency of 0.12–0.20 Hz. As shown in Fig. 4, the soft–stiff frequency range [4243] is adopted as the conventional design range for the SCHTs, which is realised by placing the first modal frequency between 1P and 3P excitation frequencies. After a minimum of 10% separation was used from the operational frequencies, the ranges of the permissible frequency can be defined as follows:

Table 1
Ranges of key tower parameters.

Concrete base diameter/d_{cb}	Concrete top diameter/d_{ct}	Concrete thickness/t_c	Steel/concrete length ratio/α_{sc}
5000–10000 mm	5000–5500 mm	200–400 mm	0.08–1.55
Adapter bottom diameter/d_{ab}	Adapter top diameter/d_{at}	Adapter thickness/t_a	Adapter height/h_a
Same with d_{ct}	400–600 mm greater than d_{sb}	1500–1800 mm	1500–2000 mm
Steel bottom diameter/d_{sb}	Steel top diameter/d_{st}	Steel bottom thickness/t_{sb}	Steel top thickness/t_{st}
$\leq$4300 mm	3300–3500 mm	$\leq$40 mm	$\leq$40 mm

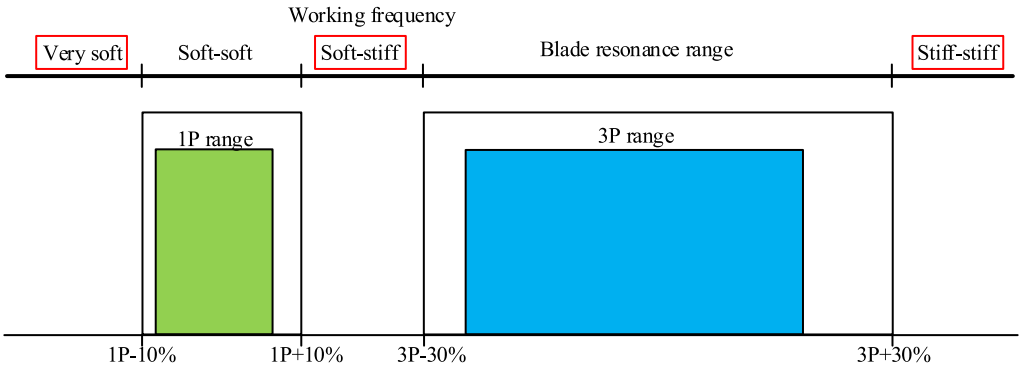

Fig. 4. Permissible frequency of the hybrid tower.

$$0.22\ \text{Hz} = f_{1p+10\%} \leqslant f_{1st} \leqslant f_{3p-30\%} = 0.32\ \text{Hz} \tag{5}$$

The Rayleigh method was previously used for estimating a tower with non-uniform flexural rigidity and mass density distribution. It is an approximate approach that primarily depends on the assumed deflection shape function. Hamilton's formulation provides the basis for accurately describing the dynamic equations of motion and can be expressed as follows:

$$\delta \int_{t_1}^{t_2} (T - U)dt = 0 \tag{6}$$

where T and V denote kinetic and potential energies of the system, respectively. Additionally, δ denotes the first variation operator, and t_1 and t_2 denote time intervals. The kinetic energy and potential energy of the tower with variable properties are then considered as follows:

$$T = \frac{1}{2}\int_0^L m(x)\left(\frac{\partial w}{\partial t}\right)^2 dx \tag{7}$$

$$V = \frac{1}{2}\int_0^L n(x)\left(\frac{\partial^2 w}{\partial x^2}\right)^2 dx \tag{8}$$

By substituting Eqs. (7) and (8) in Eq. (6), we obtain the following expression:

$$m(x)\frac{\partial^2 w}{\partial t^2} + \frac{\partial^2 n(x)}{\partial x^2}\frac{\partial^2 w}{\partial x^2} + 2\frac{\partial n(x)}{\partial x}\frac{\partial^3 w}{\partial x^3} + n(x)\frac{\partial^4 w}{\partial x^4} = 0 \tag{9}$$

After using the dot and prime notations to represent partial derivatives with respect to t and $\times$, respectively, the equation is expressed as follows:

$$m(x)\ddot{w} + n''(x)w'' + 2n'(x)w''' + n(x)w'''' = 0 \tag{10}$$

We assume that the shape of the vibration is under a simple harmonic motion, and Eq. (9) can be transformed from a partial differential equation to an ordinary differential equation. The solution of Eq. (9) is then calculated via separation of variables as follows:

$$w(x,t) = \phi(x)e^{-iwt} \tag{11}$$

The equation above represents the harmonic variation of a specific shape $\phi(x)$ with a time-dependent amplitude, in which $\phi(x)$ denotes a function of position x. We substitute this equation into Eq. (10) to obtain the following expression:

$$\left[-m(x)w^2 + n''(x)\frac{d^2}{dx^2} + 2n'(x)\frac{d^3}{dx^3} + n(x)\frac{d^4}{dx^4}\right]\phi(x) = 0 \tag{12}$$

We consider the non-uniform beam shown in Fig. 2, and its four prescribed boundary conditions at $\times = 0$ and $\times = L$ are as follows:

$$\phi(0) = \phi'(0) = \phi''(L) = 0,\ \ \frac{d}{dx}\left[n(x)\frac{d^2\phi(x)}{dx^2}\right]_{x=L} + Mw^2\phi(L) = 0 \tag{13}$$

The natural frequencies and modal shapes of the SCHT can be obtained by solving the eigenvalue of the equation using the differential quadrature method [44,45].

3.3. Deriving equations governing top deflections

Excessive tower deflection can lead to a collision between the rotating blades and face of the tower. The maximum horizontal deformation Δ_{max} and rotation θ_{max} at the tower top were typically limited to 1.25% of the tower height and 5° [46]. The tower deflections can be calculated by implementing a numerical integration, in which a linear elastic behaviour was assumed in the structure. The wind loads were considered by assuming a concentrated lateral force F_{top} and bending moment M_{top} at the top of the tower. The lateral displacement and flexural rotation at the top were derived using the virtual work principle as follows:

$$\Delta_{max} = F_{top}\left(\int_0^L \frac{\overline{M}(x)M_p(x)}{n(x)}dx\right) + M_{top}\left(\int_0^L \frac{\overline{M}(x)\cdot 1}{n(x)}dx\right) < 1.25\%L \tag{14}$$

$$\theta_{max} = \left[M_{top}\left(\int_0^L \frac{1\cdot 1}{n(x)}dx\right) + F_{top}\left(\int_0^L \frac{1\cdot M_p(x)}{n(x)}dx\right)\right]\frac{180}{\pi} < 5 \tag{15}$$

where $\overline{M}(x)$ denotes bending moment in a member owing to a unit virtual load, and $M_p(x)$ denotes bending moment produced by the unit external load.

3.4. Checking the compressive stresses of the concrete and steel towers

An increase in the bending moment that is applied to the concrete tower induces an inelastic deformation lumped to the segment-to-segment joints. This provides an advantage of decreasing damage to the adjacent segments. The normal stresses in the joints primarily correspond to three types as follows: pre-stressing, gravity, and applied loads. When there are no normal stresses at the outermost perimeter, the concrete tower does not behave in a monolithic manner. The opening of the joints can result in a significant stiffness reduction and local concrete crushing near the compressive region. Hence, gap propagation in joints affects global stability of the system and is not allowed at ULS. The minimum and maximum normal stresses of each horizontal junction should be verified via the following expressions:

$$\sigma_{min} = \frac{F_c(x) + F_{pt0}}{A_c(x)} - \frac{M_c(x)}{I_c(x)/[d_{o,c}(x)/2]} \leqslant 0 \tag{16}$$

$$\sigma_{max} = \frac{F_c(x) + F_{pt0}}{A_c(x)} + \frac{M_c(x)}{I_c(x)/[d_{o,c}(x)/2]} \leqslant 0.9\sigma_{cd}(x) \tag{17}$$

where $\sigma_{cd}(x)$ denotes concrete design compressive strength, and $F_c(x)$ and $M_c(x)$ denote total vertical force and bending moment acting on the concrete position $\times$, respectively. The tendons were placed along the

tapered tower profile. In particular, F_{pt0} denotes the vertical component of the initial PT force. The bending moment produced by the horizontal component of the tendon forces was neglected in the deformed tower because it was minimal with respect to $M_c(x)$.

The steel tower shell subjected to compression was evaluated based on the ASCE/AWEA RP2011 standard [47]. The compressive strength of the steel section was limited by

$$\frac{F_s(x)}{A_s(x)}+\frac{M_s(x)}{I_s(x)/[d_{o,s}(x)/2]}\leqslant\sigma_{sd} \tag{18}$$

where $\sigma_{sd}(x)$ denotes steel design compressive strength and corresponds to $0.9\sigma_{cr}(x)$, and $F_s(x)$ and $M_s(x)$ denote the total vertical force and bending moment acting on the steel position × , respectively. For round hollow structural sections with diameter-to-thickness ratios (λ_s) of less than 300 and greater than $0.11E_s/F_y$, the critical strength $\sigma_{cr}(x)$ is determined as follows:

$$F_{cr}=[0.038\frac{E_s}{F_y\lambda_s}+\frac{2}{3}]F_y, \text{when } 0.11\frac{E_s}{F_y}<\lambda_s\leqslant 0.357\frac{E_s}{F_y} \tag{19}$$

$$F_{cr}=0.276\frac{E_s}{\lambda_s}, \text{when } 0.357\frac{E_s}{F_y}<\lambda_s\leqslant 330 \tag{20}$$

where F_y denotes the specified minimum yield stress of the steel.

3.5. Checking the tower fatigue strength

The SCHT is a fatigue-loaded structure due to the varying nature of wind. A fatigue assessment is performed to ensure that the SCHT exhibits sufficient resistance to fatigue failure during its operational life. The fatigue loading is due to the rotating blades of the rotor under operational conditions. Given a typical 20-year service life, the design-life number of cycles N_t is as follows:

$$N_t=\eta\times n_{rated}\times(20\times 365\times 24\times 60[min]) \tag{21}$$

where n_{rated} denotes the rated rotor speed of the wind turbine, and η denotes wind availability (98.5%) at the chosen site. The resistance against fatigue of a critical component is typically expressed in terms of the fatigue life curves (S–N curves). The S–N curves were selected based on the reference report [9] and standard [48]. The number of loading cycles to failure for the steel section ($\log N_s$) and concrete section ($\log N_c$) are expressed as follows:

$$logN_s=13.9-4log\Delta S_s \tag{22}$$

$$logN_c=14\frac{1-E_{cd,max}}{\sqrt{1-\frac{E_{cd,min}}{E_{cd,max}}}} \tag{23}$$

where ΔS_s denotes the steel stress range, and $E_{cd,max}$ and $E_{cd,min}$ denote maximum and minimum concrete compressive stress levels, respectively. Fatigue damage is estimated using the Miner's rule summation. The fatigue constraint should comply with the following expression:

$$\frac{logN_t}{logN_s}-1<0 \tag{24}$$

$$\frac{logN_t}{logN_c}-1<0 \tag{25}$$

4. Sensitivity analysis of the first modal frequency

Although avoiding resonance is not a historical constraint for building-type structures, it is of primary interest for the tower because it constantly sustains operational vibrations of the turbine [49–51]. Hence, a sensitivity analysis was performed using the tower free vibration to understand the parameters that exert the highest effect on the first modal frequency of SCHTs of different heights. Classes C50 and Q355 were used to define section properties of the steel and concrete. The steel material was defined using a density of 8500 kg/m^3, Poisson's ratio of 0.3, and modulus of elasticity of 206,000 MPa. The steel density was increased from a typical value of 7850 kg/m^3 to 8500 kg/m^3 to represent paint and connections that were not considered in tower thickness data [52]. The concrete was defined using a density of 2500 kg/ m^3, Poisson's ratio of 0.2, and modulus of elasticity of 37,000 MPa. The weight of the top tower mass was considered as 250 tons for the representation of an onshore wind turbine with a capacity of 3–4 MW. The hybrid form of construction is frequently offered as an alternative to very tall towers that exceed 100 m. Hence, SCHTs with heights corresponding to 100, 120, 140, and 160 m were selected for analysis.

The Latin hypercube sampling (LHS) method can avoid clustering and therefore exhibits high efficiency in sampling. The basic idea of the LHS is inspired by the concept of "Latin square" from combinatorial mathematics [53–55]. It can stratify across the range of each sampled variable and ensure that the sampling is distributed at different levels, thus reducing the number of realizations required to maintain the probability distribution. Hence the LHS is selected to obtain 5000 groups of design parameters for each SCHT with different heights. The top sections of the concrete portion ($d_{tb}=4500$ mm, $t_{ct}=t_{cb}$), adapter ring ($d_{ab}=4500$ mm, $t_{at}=t_{ab}=1500$ mm), and steel portion ($d_{st}=3500$ mm, $t_{st}=t_{sb}$) were fixed in the sampling to avoid a tapered profile with larger top sections and smaller bottom sections. Finally, only the following design parameters were considered during model updating as follows: (1) d_{cb}, (2) t_c, (3) α_{sc}, (4) l_t, (5) t_t, (6) t_s, and (7) d_{sb}. Furthermore, adjustments to the concrete length l_c were adopted to account for the effects of the steel/concrete height ratio α_{sc}. All random variables are considered as independent and are assumed to obey a uniform distribution function. The ranges of parameter d_{cb}, which were selected for SCHTs of different heights to maintain the first modal frequency in the prescribed range, are presented in Table 2. The upper and lower bounds of the other parameters are listed in Table 1.

The variables in the steel portion and transition portion exert a lower impact on the first bending mode than those of the concrete portion, as shown in Fig. 5. The first three important variables correspond to parameters l_c, t_{cb}, and t_{sb}. The most important variables with respect to the first modal frequency vary as tower height increases. The first modal frequency is most sensitive to parameter l_c for taller towers. However, linear correlation coefficients decrease by 4.1 %, 15.4 %, and 103.7 % when total tower height decrease from 160 m to 140 m, 120 m, and 100 m, respectively. For the 100 m high tower, the main effect on the first modal frequency was due to parameters t_{cb} and d_{cb}. The highest positive linear correlation coefficient was 0.6 for parameter t_{cb}. The comparisons suggested that when concrete is used as a partial replacement for steel in the lower tower sections, its efficiency increases with the tower height.

To provide insights into the effects of geometric parameters in the concrete portion, rigorous parametric analyses are conducted with respect to four different height, as listed in Table 3. When the identified parameters were investigated for each ease, other parameters remained constant.

Figures 6 and 7 show the variation in the first modal frequency with respect to parameters α_{sc}, t_{cb}, and d_{cb}. Grey points denote the results of the sensitivity analysis and are presented for comparison. The non-monotonic dependence of the first modal frequency on parameter α_{sc} can be counterintuitive, thereby indicating that increases in the proportion of concrete on the tower height can decrease the first modal frequency. The frequency of vibration for any mode is related to the generalised stiffness ($k^*=\sum n(x)[\varphi''(\xi)]^2\Delta x$) and generalised mass ($m^*$

Table 2
Ranges of parameter d_{cb} used in the sensitivity analysis.

160 m	140 m	120 m	100 m
9000–10000 mm	8000–9000 mm	7000–8000 mm	4500–5500 mm

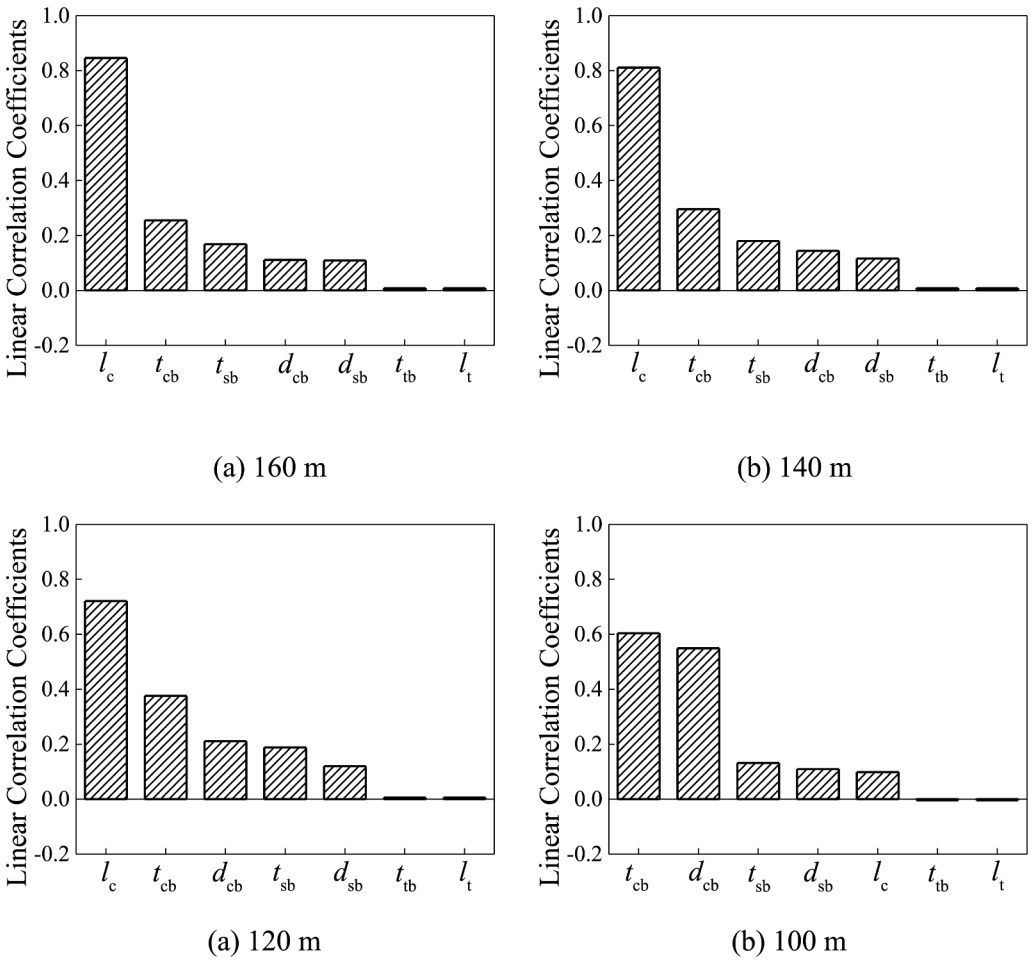

Fig. 5. Linear correlation coefficients between design variables and the first modal frequency.

Table 3
Key dimensions of four examples.

Concrete portion				Adapter ring				Steel portion				Height/m
Base/mm		Top/mm		Base/mm		Top/mm		Base/mm		Top/mm		
d_{cb}	t_{cb}	d_{ct}	t_{ct}	d_{ab}	t_{ab}	d_{at}	t_{at}	d_{sb}	t_{sb}	d_{st}	t_{st}	H
5000	200	4500	200	4500	1500	4500	1500	4300	25	3500	25	100
7000	200	4500	200	4500	1500	4500	1500	4300	25	3500	25	120
9000	300	4500	300	4500	1500	4500	1500	4300	25	3500	25	140
10,000	300	4500	300	4500	1500	4500	1500	4300	25	3500	25	160

$= \sum m(x)[\varphi(\xi)]^2\Delta x + M[\varphi(L)]^2$), and thus, a detailed investigation of k^* and m^* is required to elucidate the counterintuitive result of SCHTs. We consider SCHTs with heights of 100 m ($d_{cb} = 4500$ mm in Fig. 7d) and 160 m ($d_{cb} = 9500$ mm in Fig. 7a) as examples. The significant difference between the two SCHTs, as shown in Fig. 8, corresponds to the variation in k^* and m^* with respect to parameter α_{sc}. A significant increase in m^* is observed when parameter α_{sc} decreases to a certain level whereas k^* is approximately linear with parameter α_{sc}. Thus, this indicates that adoption of concrete in the upper sections leads to a disproportionate amount of bending stiffness relative to the increasing tower weight. The phenomenon subsequently caused the first modal frequency to initially increase and then decrease with decreases in α_{sc}. Moreover, for the 160 m high SCHT, the generalised stiffness increased by 2.18 times when parameter α_{sc} was varied from 1.51 to 0.10. Correspondingly, the generalised stiffness of the 100 m high SCHT increased by 0.04 times. This difference suggests that the contribution of the proportion of concrete to the generalised stiffness of SCHTs significantly decreases as tower height decreases.

Furthermore, other important observations from Figs. 6–7 are as follows: (a) An increase in parameter d_{cb} leads to a varied effect on the first modal frequency in the different α_{sc} ranges. An increase in parameter d_{cb} by 1000 mm for the 160 m high SCHT leads to an increase in the first modal frequency by 25.8 % for $\alpha_{s\ c} = 0.10$ and by 13.1 % for $\alpha_{sc} = 1.51$. Correspondingly, for the 100 m high SCHT, the first modal frequency increases by 66.1% and 102.6%, for $\alpha_{sc} = 0.10$ and for $\alpha_{sc} = 1.51$, respectively. (b) In contrast to increases in parameter d_{cb}, results indicate that the advantage of parameter t_c on the first modal frequency decreases when parameter t_c continuously increases. The peak values of SCHTs with heights of 160, 140, 120, and 100 m increased by 14.4 %, 14.8 %, 15.5 %, and 15.5 %, respectively, when parameter t_{cb} varied from 200 mm to 300 mm and increased by 8.8%, 9.1%, 9.4%, and 9.4%, respectively, when parameter t_{cb} varied from 300 mm to 400 mm. (c) An increase in tower height leads to an increase in the probability of exceeding the lower bound of the first modal frequency in the current

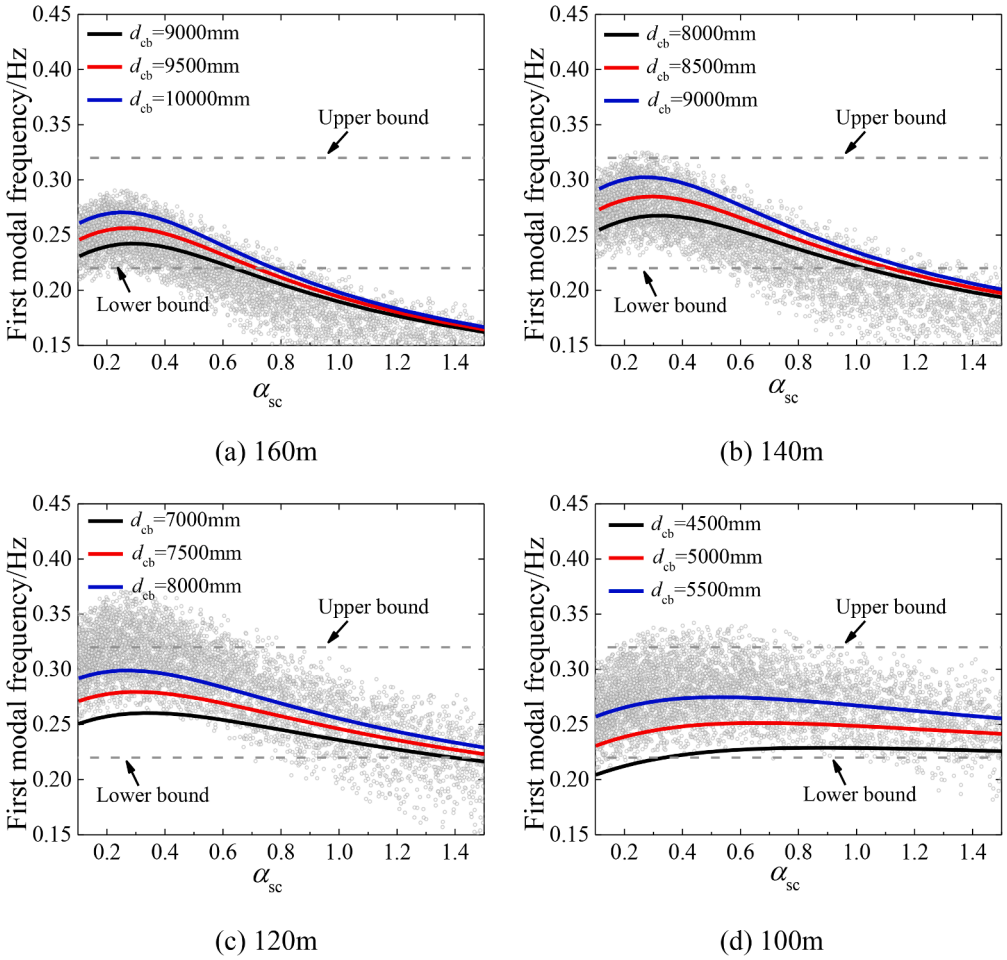

Fig. 6. Variations in the first modal frequency with respect to parameters α_{sc} and d_{cb}.

design space. For the 160 m high SCHT with $d_{cb} = 9000$ mm, the tower satisfies the frequency limit until parameter α_{sc} is lower than 0.6. (d) A significant difference was observed in the variation of the first modal frequency when parameter α_{sc} changed for SCHTs of different heights. In particular, the 100 m high SCHT exhibited a slight variation in the first modal frequency with respect to parameter α_{sc} when compared to that of towers with heights exceeding 120 m. This indicated good consistency with the results of the sensitivity analysis.

5. Geometric optimisation using a genetic algorithm

A case study is used to illustrate the geometric optimisation of the SCHTs. A 160 m tower with a top mass of 250 tons was selected as an example due to its higher sensitivity to the proportion of concrete. The design compressive strength of C50 used for the concrete part was 33.3 MPa [56]. The nominal yield strength of Q355 used for the steel part was 355 MPa. The allowable steel stress was 323 MPa considering the partial safety factor for materials [40]. The tendons were analysed using a Poisson's ratio of 0.3, modulus of elasticity of 196000 MPa, and limited stress of 1200 MPa [57]. In addition to gravity, towers are mainly designed to withstand two types of loads: those resulting from the rotating blades and those acting on the tower. The former is the dominant load in the operational scenario (i.e., mainly lateral forces and bending moments acting on the top of the tower), while the latter is a non-uniform distributed load over the length of the tower. For simplicity, the base shear contributed by the latter was conservatively converted into a point load located at the top of the tower. The total equivalent loads in the fatigue and ultimate load cases obtained from wind turbine manufacturing are listed in Table 4. Note that an iterative design is required when there is a big difference between the loads at the initial loading stage and the loads obtained from the dynamic analyses.

Different algorithms have been developed to perform structural optimisation [58–65], thus providing an opportunity for rapidly determining the optimised geometry of the SCHT. A genetic algorithm (GA), implemented in MATLAB, was selected as the optimisation method in this study. The GA is a stochastic algorithm that commences by creating a random initial population and then computes the next population using individuals in the current generation. At each step, the GA creates three types of children by: (a) automatically surviving the individuals with best fitness values to the next population (Elite), (b) making random changes to a single parent (Mutation) and (c) combining the vectors of parents (Crossover). The default options were used to define the optimisation task with the exception that the population size and maximum number of iterations were varied. With a large population size and maximum number of iterations, the GA is slower although it can perform a more thorough search of the solution space, thereby increasing the probability of returning a global minimum. The objective of the optimisation was to adjust the design parameters to maximise the cost-effectiveness of the SCHTs. After simplifying the cost of different tower components as fixed, the objective function is expressed as follows:

$$C_{obj} = P_{ct}V_{ct} + P_{ca}V_{ca} + P_{st}M_{st} + P_{ps}L_p + P_{ec}L_c + P_{es}L_s \tag{26}$$

where P_{ct}, P_{ca}, P_{st}, and P_{ps} denote average unit prices of the concrete tower, concrete adapter, steel tower, and PT tendons, respectively. Additionally, P_{ec} and P_{es} denote average unit prices for erecting concrete

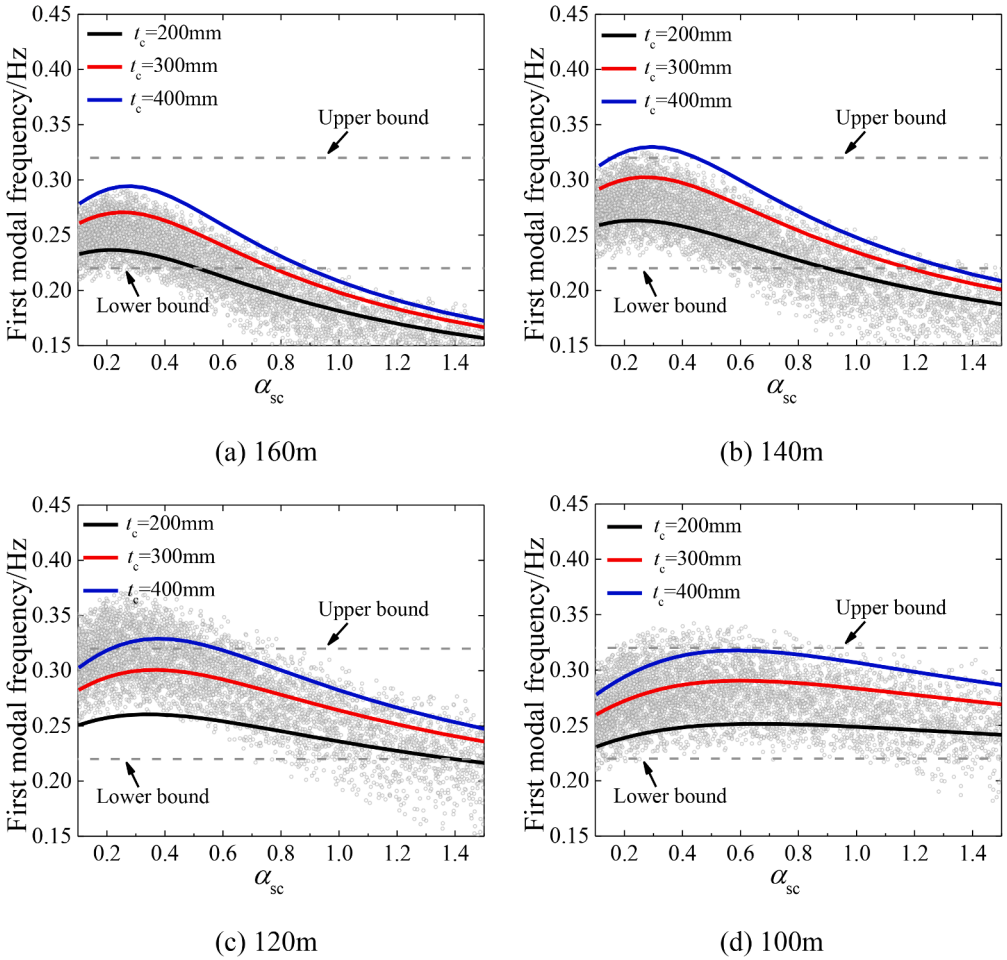

Fig. 7. Variations in first modal frequency with respect to parameters α_{sc} and t_c.

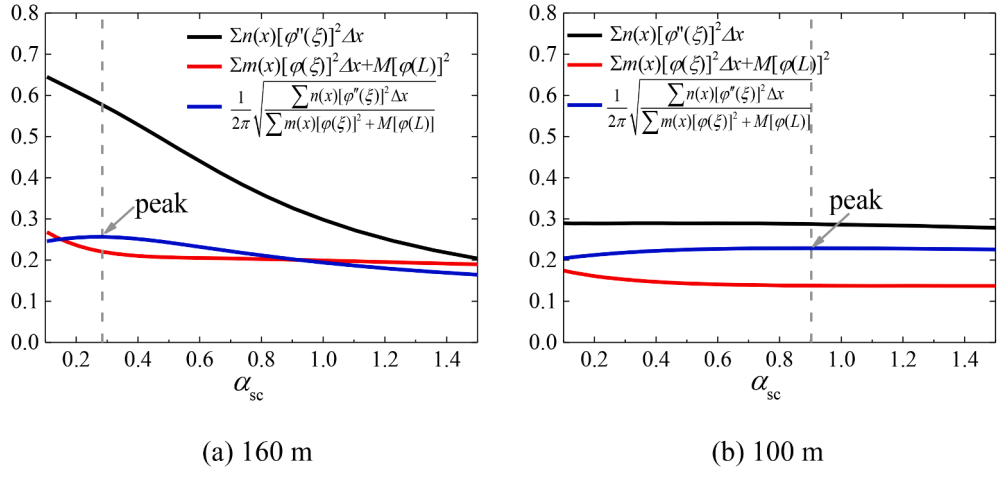

Fig. 8. Comparison of generalised stiffness and generalised mass with respect to parameter α_{sc}.

Table 4
Static equivalent top loads.

Fatigue loads		Ultimate loads	
$F_{top,f}$/N	$M_{top,f}$/N•m	$F_{top,u}$/N	$M_{top,u}$/N•m
4×10^5	5×10^7	1×10^6	5×10^9

and steel towers, respectively. Furthermore, V_{ct} and V_{ca} denote total volumes of the concrete tower and adapter ring, respectively, and M_{st} denotes the total weight of the steel tower. Moreover, L_p, L_c, and L_s denote lengths of the 140 mm^2 cross-sectional high-strength strands, concrete tower, and steel tower, respectively. The reference costs of different tower components, such as those collected from wind turbine companies in China, are listed in Table 5. The unit prices of ¥3000/m^3 and ¥6000/m^3 exceeded the typical material price of concrete to account

Table 5
Average unit costs of different tower components.

P_{ct}	P_{ca}	P_{st}	P_{ps}	P_{ec}	P_{es}
¥3000/m^3	¥6000/m^3	¥9000/ton	¥20/m	¥5500/m	¥500/m

for supplemental costs of reinforcement, labour, machining, and maintenance. To provide realistic cost assumptions for the steel tower and PT strands, the unit price of ¥9000/ton included costs of paint and connections, and the unit price of ¥20/m incorporated costs of the anchorage and prestress process. Concrete towers involve a low material cost although their installation requires larger cranes and higher labour costs when compared to those of the steel tower. In particular, unit prices of ¥5500/m and ¥500/m were determined by considering differences in the lifting duration and apparatus of the concrete and steel towers.

The proposed equations were expressed as an array of nonlinear inequality constraints to ensure structural responses within the prescribed limits. They were programmed in a consistent format, $c(:,x) < 0$ by obtaining the expressions on the left-hand side, and thereby making the inequality into less than form. As the tower parameters are adjusted in each step, the constraint conditions are indirectly updated automatically, and thus, the parameters can be rapidly weighed based on the response. The thickness and height of the concrete adapter were conservatively set as fixed values ($t_a = 1800$ mm and $h_a = 2000$ mm) to decrease the dimensionality of the optimisation problem. The diameter and thickness of the concrete and steel towers varied linearly from the base to the top to offer low material quantities.

The GA ran for (1) 100 generations with each including 300 individuals and for (2) 150 generations with each including 200 individuals. The other parameters defining the GA are summarized in Table 6. Parallel computations consisting of 12 processors were used to speed up the optimization process. In addition to parallel computations, the computational efficiency was also improved by adopting an upper bound strategy (UBS) or seeding the initial population with feasible solutions. The aim of the UBS was to detect the children having no chance to surpass the current best design and exclude them from the structural analysis. The initial population could be chosen from a final population in a previous run if a better result was expected. More details about the two methods were given in the existing literature [66–68].

The evolution of the optimal individual cost over generations is shown in Fig. 9 and tabulated in Table 7. Different convergence curves realise a similar final optimal value. The computing time of two runs are 5877 s and 5912 s, respectively. The final optimal solution shows a 12.7% lower cost than the initial design while satisfying all the design constraints. The corresponding design parameter values are listed in Table 8. The parameters denote an SCHT comprising an 11.7 m steel part at the top and a 146.3 m concrete part at the bottom. Parameters l_c and d_{cb} were optimised to approximate or realise their upper bounds during optimisation. This suggests that by increasing parameters l_c and d_{cb}, a more significant effect is induced on the structural response when compared to that due to the other parameters. The first modal frequency was approximately 0.240 Hz, which was within the desired range of 0.22–0.32 Hz. The top lateral deformation and rotation were 804 mm and 0.6°, respectively, which were considerably below the corresponding limits. The accumulated damage of the steel and concrete towers ranged from 0.0 to 0.99. Furthermore, values less than or equal to 1 indicated adequate fatigue strength for the tower over the design

Table 6
Parameters for defining the GA.

Crossover Fraction	Mutation Fcn	Elite Count	Constraint Tolerance	Function Tolerance
0.8	Mutationgaussian Scale = 1; Shrink = 1	5%	1E-3	1E-6

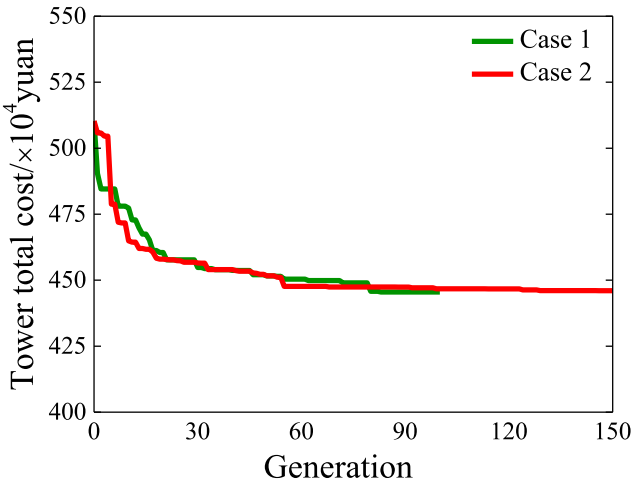

Fig. 9. Convergence plot of the GA.

Table 7
Comparison of statistical results in two runs.

Design case	Initial optimised cost/ ×10^{4}yuan	Final optimised cost/ ×10^{4}yuan	Computing time/s
Case1	510.1	445.5	5877
Case2	510.3	446.0	5912

lifetime of a turbine. The results of the compressive strength in concrete and steel towers are shown in Figs. 10–11. The most saturated constraints for the absolute minimum stress were observed at the concrete base. The compressive stresses of different steel sections only corresponded to 21–31% of their upper bounds.

A 3D finite-element model was created using ABAQUS [69] based on the best design solution. The simulation was conducted to validate the equations derived for the frequency constraint, top deflection constraint, and compressive stress constraint for the concrete portion. As shown in Fig. 12, the entire SCHT is supported on a rigid foundation. The concrete tower and adapter ring were modelled as reduced integration solid elements (C3D8R), and the steel tower was modelled as reduced integration shell elements (S4R). The entire mesh was selected to balance a sufficiently accurate output relative to reasonable computation efforts. Three tower portions were meshed in a similar manner along the height and diameter of the tower using an approximate global size of 200 mm. The concrete tower approximately included three elements along the thickness to capture the bending effect. The PT strands are placed to follow the elevation of the inner tower wall, depending on the tower geometry. They are modelled as two-node truss elements with the top and bottom nodes anchored to the transition portion and foundation via a kinematic coupling constraint applied to the hole edges. The initial prestress in the strands was determined by applying a temperature variation.

The concrete tower was assumed to include 10 concrete segments, and the steel tower was assumed to comprise five segments welded together. The thickness of each segment was simplified as a constant and equal to its maximum value. The joints between adjacent concrete segments were modelled with hard contact, thereby indicating that geometric nonlinearity resulting from the opening of these interfaces is included. The welded joints between the steel sections and connection between the steel tower and adapter ring were modelled via tie constraints. Three analysis steps are adopted to represent the construction and loading sequence as follows: (1) strand initial stress, (2) free vibration, and (3) lateral loading. The lateral load and top combined mass were applied at a reference node that was coupled to the region of the top tower surface.

Table 8
Final optimised design for the tower geometry.

d_{cb}/m	t_{cb}/mm	d_{ct}/m	t_{ct}/mm	d_{sb}/m	t_{sb}/mm	d_{st}/m	t_{st}/mm	l_c/m	F_{pt0}/MN
10.00	228	5.12	245	4.00	30.9	3.36	13.1	146.3	46.3

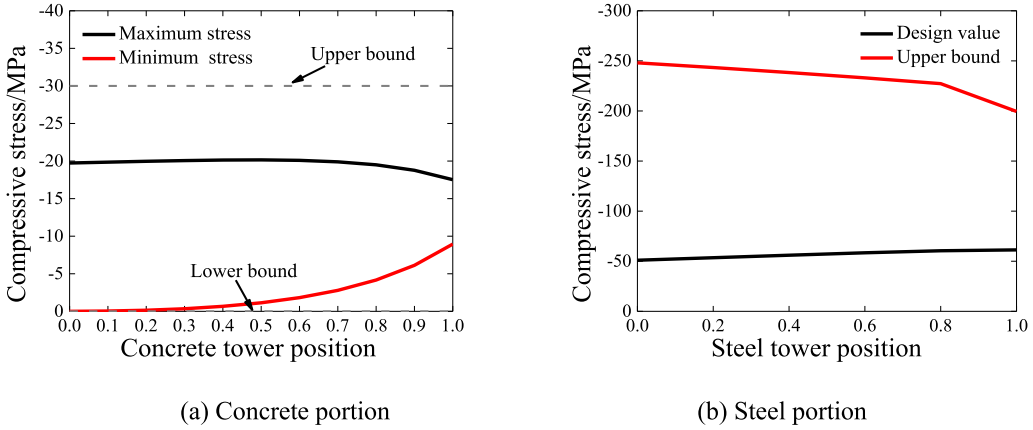

(a) Concrete portion (b) Steel portion

Fig. 10. Compressive stress distribution of the tower.

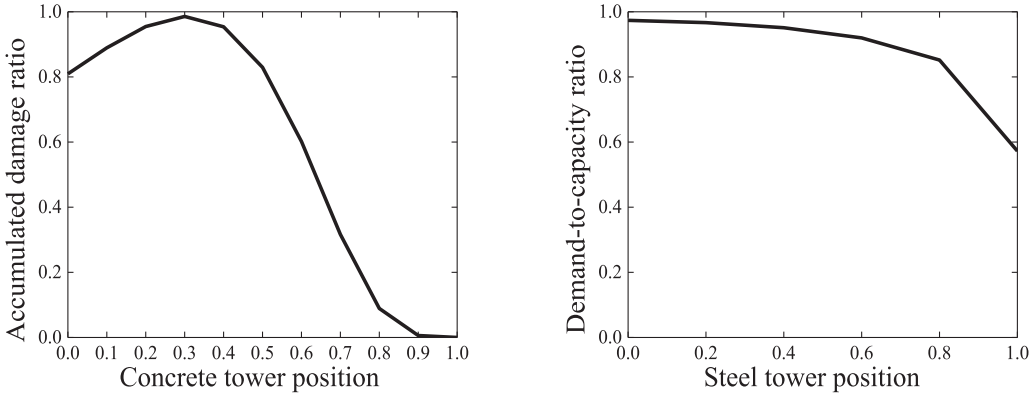

(a) Concrete portion (b) Steel portion.

Fig. 11. Accumulated damage distribution of the tower.

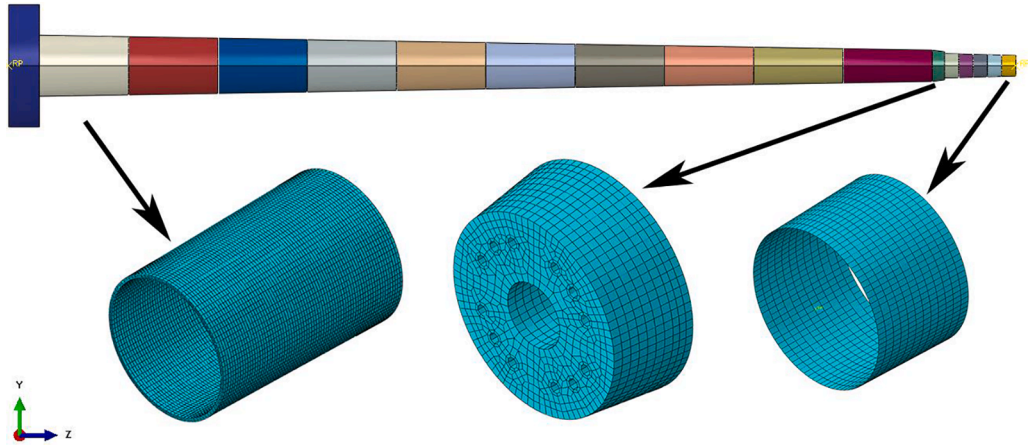

Fig. 12. Finite element model of the hybrid tower.

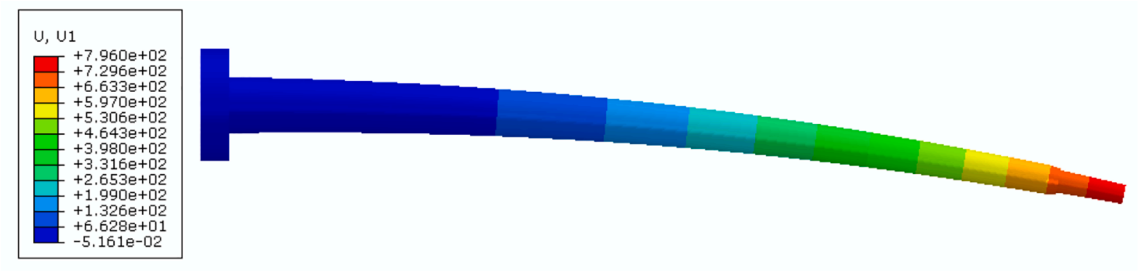

(a) Lateral deformation distribution of the complete model

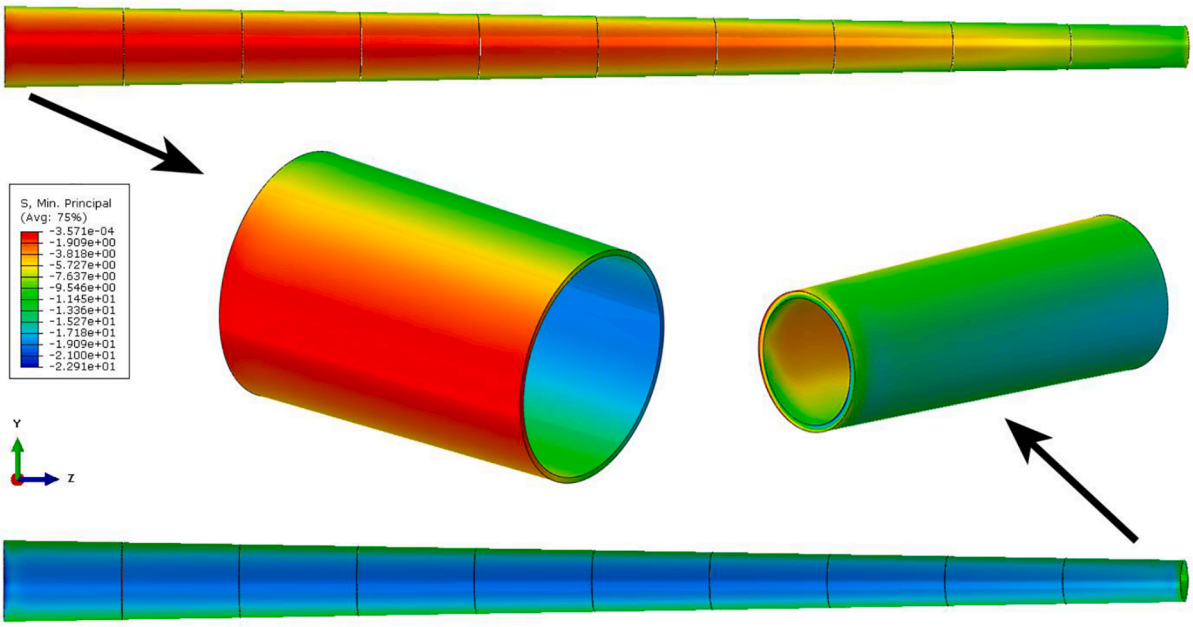

(b) Minimum principal stress for the concrete portion

Fig. 13. Contour plots of FEM at maximum lateral loading.

The first modal frequency of the FEM (0.240 s) was in good agreement with theoretical values (0.241 s), thereby indicating that the equations can predict the first modal frequency. As shown in Fig. 13(a), maximum deformation of the structure is observed at the top of the tower with a value corresponding to 796 mm, which is slightly lower than the predicted value of 804 mm. The small difference can be attributed to the contributions of the strands and stepped tower sections in the FEM. The profiles of the compressive stress along the height of the concrete portion are determined as similar by comparing simulated results in Fig. 13(b) and derived results in Fig. 10(a). The minimum absolute value was observed at the tower base. The value was approximately equal to zero, which was in good agreement with the predicted value. The main difference in the simulation corresponded to the compressive stress at the top surface of the concrete portion, thereby demonstrating a non-uniform stress distribution along the tower thickness. The discrepancy was mainly attributed to the inability of the equations to capture possible local events.

6. Conclusions

In this study, an optimisation framework based on five design constraints was developed as a replacement for an FEM to determine the optimal geometry of steel–concrete hybrid towers (SCHTs). The geometric constraint was determined based on manufacturing and transport limitations. The frequency constraint was applied by deriving governing partial differential equations of motion using Hamilton's principle. The compressive stress constraint for the precast concrete tower was determined via the compressive resistance of horizontal segment-to-segment joints. The compressive stress constraint for the steel tower and fatigue constraint were included based on the requirements of reference standards. The top deflection constraint was applied using the virtual work principle.

Frequency constraint typically corresponds to the primary constraint in wind turbine tower design. A sensitivity analysis was conducted to investigate the effects of different geometric parameters on the first modal frequency of towers with 160, 140, 120, and 100 m heights. The results indicated that decreasing in the heights of the towers from 160 m to 140, 120 and 100 m decreased the sensitivity of the first modal frequency to the concrete tower height by 4.1 %, 15.4 %, and 103.7 %. Additionally, the first modal frequency did not always increase as the proportion of concrete increased. This is because the adoption of concrete in the upper sections provided a disproportionate amount of bending stiffness with respect to the increasing tower weight.

Given the contribution of the concrete portion to the first modal frequency of taller towers, a 160 m high tower was selected to verify expected optimisation from the proposed framework. A genetic algorithm (GA) was used as the optimisation method. Parallel computations consisting of 12 processors were used to speed up the optimization task. The computing time of two runs are 5877 s and 5912 s, respectively. The final optimised solution indicated a decrease in tower cost by 12.7% and

all the design constraints were satisfied. The concrete tower height and its base diameter approximated or reached their upper bounds. In particular, first modal frequency, fatigue strength, and minimum compressive strength at bottom concrete sections were very close to the limits, thereby indicating that they corresponded to governing constraints in the design. The results of the derived equations in this case study were finally validated via 3D finite element models.

Declaration of Competing Interest

The authors declare that they have no known competing financial interests or personal relationships that could have appeared to influence the work reported in this paper.

Acknowledgements

The authors gratefully acknowledge the financial support provided by 'Fok Ying Tung Education Foundation' (171066), 'National Natural Science Foundation of China' (52008056 and 51822804), 'China National Postdoctoral Program for Innovative Talents' (BX20200071), 'China Postdoctoral Science Foundation' (2020M673140), and 'Chongqing Postdoctoral Science Foundation' (cstc2020jcyj-bshX0076). The authors would also like to thank Mr Wei Luo of CSIC HaiZhuang Wind power Co.,Ltd and Mr Dongliang Zhang of POWERCHINA Hua-Dong Engineering Co.,Ltd for their assistance with on-site photos and field survey.

References

[1] Blanco MI. The economics of wind energy. Renew Sustain Energy Rev 2009;13(6–7):1372–82.
[2] Neto JXV, Junior EJG, Moreno SR, et al. Wind turbine blade geometry design based on multi-objective optimization using metaheuristics. Energy 2018;162:645–58.
[3] Harrison R, Hau E, Snel H. Large wind turbines design and economics. New York, NY: John Wiley & Sons Ltd; 2000.
[4] McKenna R, vd Leye PO, Fichtner W. Key challenges and prospects for large wind turbines. Renew Sustain Energy Rev 2016;53:1212–21.
[5] Lantz E, Roberts O, Nunemaker J, et al. Increasing wind turbine tower heights: Opportunities and challenges. Report, National Renewable Energy Laboratory, Golden, CO. 2019.
[6] Agbayani NA, Vega RE. The rapid evolution of wind turbine tower structural systems: a historical and technical overview. Struct Congress 2012:1201–12.
[7] Kaltschmitt M, Streicher W, Wiese A. Renewable energy: technology, economics and environment. Berlin: Springer; 2007.
[8] Bernuzzi C, Crespi P, Montuori R, et al. Resonance of steel wind turbines: problems and solutions. Structures 2021;32:65–75.
[9] Lanier MW. Evaluation of design and construction approaches for economical Hybrid steel/concrete wind turbine towers. Technical Report. Golden: National Renewable Energy Laboratory, 2005.
[10] Tricklebank AH, Halberstadt PH. Concrete towers for onshore and offshore wind farms technical report. Camberley: The concrete Center; 2007.
[11] Veljkovic M, Limam M, Heistermann T, Rebelo C, Simões da Silva L. Feasibility study of friction connection in tubular towers for wind turbines. In: SSCS2010–international symposium on steel structures: culture & sustainability 2010, Istanbul, Turkey; 2010. p. 381–8.
[12] Engström S, Lyrner T, Hassanzadeh M, Stalin T, Johansson J. Tall towers for large wind turbines, Report from Vindforsk project V-342 Högatorn för vindkraftverk, Elforsk rapport 10:48, Sweden, July 2010; 2010.
[13] Lotfy I. Prestressed Concrete Wind Turbine Supporting System, Master dissertation, College of Engineering, University of Nebraska, Lincoln, Nebraska; 2012.
[14] Quilligan A, O'Connor A, Pakrashi V. Fragility analysis of steel and concrete wind turbine towers. Eng Struct 2012;36:270–82.
[15] Wu XG, Yang J, Mpalla IB. Innovative Post-tensioned hybrid wind turbine tower made of ultra high performance cementitious composites segment. ASEM13. Jeju, Korea, 2013.
[16] Rebelo C, Moura A, Gervásio H, et al. Comparative life cycle assessment of tubular wind towers and foundations–Part 1: structural design. Eng Struct 2014;74:283–91.
[17] Sritharan S. Wind turbine towers: precast concrete Hexcrete may help increase renewable energy capacity with taller hub height. PCI J 2015;60(6):33.
[18] Nezamolmolki D, Shooshtari A. Investigation of nonlinear dynamic behavior of lattice structure wind turbines. Renew Energy 2016;97:33–46.
[19] Gkantou M, Martinez-Vazquez P, Baniotopoulos C. On the structural response of a tall hybrid onshore wind turbine tower. Procedia Eng 2017;199:3200–5.
[20] Deng R, Zhou XH, Deng XW, et al. Compressive behaviour of tapered concrete-filled double skin steel tubular stub columns. J Constr Steel Res 2021;184:106771.
[21] Paredes JA, Barbat AH, Oller S. A compression–tension concrete damage model, applied to a wind turbine reinforced concrete tower. Eng Struct 2011;33(12):3559–69.
[22] Ghaemmaghami A, Kianoush R, Yuan XX. Numerical modeling of dynamic behavior of annular tuned liquid dampers for applications in wind towers. Comput-Aided Civ Infrastruct Eng 2013;28(1):38–51.
[23] Kenna A, Basu B. A finite element model for pre-stressed or post-tensioned concrete wind turbine towers. Wind Energy 2015;18(9):1593–610.
[24] Ma HW, Meng R. Optimization design of prestressed concrete wind-turbine tower. Sci China Technol Sci 2014;57(2):414–22.
[25] Asareh MA, Schonberg W, Volz J. Fragility analysis of a 5-MW NREL wind turbine considering aero-elastic and seismic interaction using finite element method. Finite Elem Anal Des 2016;120:57–67.
[26] Chen J, Li J, Wang D, et al. Seismic response analysis of steel–concrete hybrid wind turbine tower. J Vib Control 2021: 10775463211007592.
[27] de Lana JA, Júnior PAAM, Magalhães CA, et al. Behavior study of prestressed concrete wind-turbine tower in circular cross-section. Eng Struct 2021;227:111403.
[28] Alvarez-Anton L, Koob M, Diaz J, et al. Optimization of a hybrid tower for onshore wind turbines by Building Information Modeling and prefabrication techniques. Visualiz Eng 2016;4(1):1–9.
[29] Yoshida S. Wind turbine tower optimization method using a genetic algorithm. Wind Eng 2006;30(6):453–69.
[30] Uys PE, Farkas J, Jármai K, van Tonder F. Optimisation of a steel tower for a wind turbine structure. Eng Struct 2007;29(7):1337–42.
[31] Silva MA, Arora JS, Brasil RM. Formulations for the optimal design of RC wind turbine towers. Eng Optim 2008.
[32] Karpat F. A virtual tool for minimum cost design of a wind turbine tower with ring stiffeners. Energies 2013;6(8):3822–40.
[33] Lagaros ND, Karlaftis MG. Life-cycle cost structural design optimization of steel wind towers. Comput Struct 2016;174:122–32.
[34] Gentils T, Wang L, Kolios A. Integrated structural optimisation of offshore wind turbine support structures based on finite element analysis and genetic algorithm. Appl Energy 2017;199:187–204.
[35] Đorđević A, Đurišić Ž. Genetic algorithm based optimized model for the selection of wind turbine for any site-specific wind conditions. Energy 2021;121476.
[36] Dawood H, ElGawady M, Hewes J. Behavior of segmental precast posttensioned bridge piers under lateral loads. J Bridge Eng 2012;17(5):735–46.
[37] Li Y, Li J, Shen Y. Quasi-static and nonlinear time-history analyses of post-tensioned bridge rocking piers with internal ED bars. Structures. 2021, 32: 1455-1468.
[38] DNV-Risø, Guidelines for Design of Wind Turbines, Denmark, 2002.
[39] DNVGL-ST-0126: Support structures for wind turbines. Oslo, Norway: DNV, 2016.
[40] IEC 61400–1. Wind turbines-Part 1: design requirements. 3rd ed. Geneva, Switzerland: International Electrotechnical Commission; 2005.
[41] IEC 61400-6: Wind energy generation systems- Part6: Tower and foundation design requirements. International Electrotechnical Commission, Geneva, Switzerland. 2020.
[42] Damiani RR. Design of offshore wind turbine towers. Offshore Wind Farms. Woodhead Publishing, 2016: 263-357.
[43] Ko YY. A simplified structural model for monopile-supported offshore wind turbines with tapered towers. Renew Energy 2020;156:777–90.
[44] Clough RW, Penzien J. Dynamics of structures. 2nd Ed. New York: McGraw-Hill; 1993.
[45] Shu C. Differential quadrature and its application in engineering. Springer Science & Business Media; 2012.
[46] Nicholson JC. Design of wind turbine tower and foundation systems: optimization approach. M.Sc.thesis. Iowa: University of Iowa, 2011.
[47] ASCE/AWEA, Recommended practice for compliance of large land-based wind turbine support structures, American Society of Civil Engineers/American Wind Energy Association; Reston, USA, 2011.
[48] CEN. EN 1992-2, Eurocode 2 — design of concrete structures – concrete bridges – design and detailing rules. Brussels: CEN European Committee for Standardization; 2005.
[49] Murtagh PJ, Basu B, Broderick BM. Simple models for natural frequencies and mode shapes of towers supporting utilities. Comput Struct 2004;82(20–21):1745–50.
[50] Andersen LV, Vahdatirad MJ, Sichani MT, et al. Natural frequencies of wind turbines on monopile foundations in clayey soils—A probabilistic approach. Comput Geotech 2012;43:1–11.
[51] Zania V. Natural vibration frequency and damping of slender structures founded on monopiles. Soil Dyn Earthquake Eng 2014;59:8–20.
[52] Jonkman J, Butterfield S, Musial W, Scott G. Definition of a 5-MW reference wind turbine for offshore system development Technical Report No NREL/TP-500-38060. Golden (CO): National Renewable Energy Laboratory; 2009.
[53] McKay MD, Conover WJ, Beckman RJ. A comparison of three methods for selecting values of input variables in the analysis of output from a computer code. Technometrics 1979;21(2):239–45.
[54] Olsson AMJ, Sandberg GE. Latin hypercube sampling for stochastic finite element analysis. J Eng Mech 2002;128(1):121–5.
[55] Sheikholeslami R, Razavi S. Progressive Latin Hypercube Sampling: An efficient approach for robust sampling-based analysis of environmental models. Environ Modell Software 2017;93:109–26.
[56] CEN. EN 1992-1. Eurocode 2: design of concrete structures-part 1–1: general rules and rules for buildings. Brussels: CEN European Committee for Standardization; 2004.

[57] Huang X, Zhou Z, Eatherton MR, Zhu D, Guo C. Experimental investigation of self-centering beams for moment-resisting frames. J Struct Eng 2020;146(3):04019214. https://doi.org/10.1061/(ASCE)ST.1943-541X.0002530.
[58] Kaveh A, Mahdavi VR, Kamalinejad M. Optimal design of the monopole structures using the CBO and ECBO algorithms. Period Polytechn Civ Eng 2017;61(1):110–6.
[59] Kaveh A, Sabeti S. Optimal design of jacket supporting structures for offshore wind turbines using CBO and ECBO algorithms. Period Polytechn Civ Eng 2018;62(3):545–54.
[60] Kaveh A, Sabeti S. Structural optimization of jacket supporting structures for offshore wind turbines using colliding bodies optimization algorithm. Struct Des Tall Special Build 2018;27(13):e1494.
[61] Kaveh A, Sabeti S. Optimal design of monopile offshore wind turbine structures using CBO, ECBO, and VPS algorithms. Sci Iran Trans A, Civ Eng 2018;26(3):1232–48.
[62] Kaveh A, Sabeti S. Optimal design of jacket supporting structures for offshore wind turbines using enhanced colliding bodies optimization algorithm. Int J Optim Civ Eng 2019;9(1):129–45.
[63] Kazemzadeh AS, Kazemzadeh AS, Hasançebi O. Structural optimization using big bang-big crunch algorithm: a review. Int J Optim Civ Eng 2016;6:433–45.
[64] Azad SK. Enhanced hybrid metaheuristic algorithms for optimal sizing of steel truss structures with numerous discrete variables. Struct Multidiscip Optim 2017;55(6):2159–80.
[65] Azad SK. Design optimization of real-size steel frames using monitored convergence curve. Struct Multidiscip Optim 2021;63(1):267–88.
[66] Azad SK, Hasançebi O. Upper bound strategy for metaheuristic based design optimization of steel frames. Adv Eng Softw 2013;57:19–32.
[67] Azad SK, Hasançebi O, Azad SK, Erol OK. Upper bound strategy in optimum design of truss structures: a big bang-big crunch algorithm based application. Adv Struct Eng 2013;16(6):1035–46.
[68] Azad SK. Seeding the initial population with feasible solutions in metaheuristic optimization of steel trusses. Eng Optim 2018;50(1):89–105.
[69] ABAQUS version 2019 [Computer software]. Hibbitt, Karlsson & Sorensen, Inc., Pawtucket, RI.